1826 *Inorg. Chem.* **2010**, *49*, 1826–1833
DOI: 10.1021/ic9021867

Inorganic Chemistry
Article

3d−3d−4f Chain Complexes Constructed Using the Dinuclear Metallacyclic Complex $[Ni_2(mbpb)_3]^{2-}$ [H_2mbpb = 1,3-Bis(pyridine-2-carboxamide)benzene] as a Ligand: Synthesis, Structures, and Magnetic Properties

Enrique Colacio,*,† María A. Palacios,† Antonio Rodríguez-Diéguez,† Antonio J. Mota,† Juan Manuel Herrera,† Duane Choquesillo-Lazarte,‡ and Rodolphe Clérac*,§,⊥

†*Departamento de Química Inorgánica, Universidad de Granada, Avenida Fuentenueva s/n, 18071 Granada, Spain,* ‡*Laboratorio de Estudios Crystalográficos, IACT−CSIC, E-18100 Granada, Spain,* §*CNRS, UPR 8641, Centre de Recherche Paul Pascal, Equipe "Matériaux Moléculaires Magnétiques", 115 avenue du Dr. Albert Schweitzer, Pessac F-33600, France, and* ⊥*Université de Bordeaux, UPR 8641, Pessac F-33600, France*

Received November 5, 2009

A series of one-dimensional Ni_2Ln cationic complexes have been prepared by assembling the in situ generated dinuclear mesocate $[Ni_2(mbpb)_3]^{2-}$ building block [H_2mbpb is the ligand 1,3-bis(pyridine-2-carboxamide)benzene] with Ln^{3+} metal ions (Ln^{3+} = Gd, Tb, Dy). The crystal-field potentials for the two types of site symmetries found for these 3d−3d−4f complexes (LnO_7 and LnO_8) are quite different, which has a direct influence on the depopulation of the Stark sublevels, the magnetic anisotropy, and the magnetic properties.

Introduction

The field of molecular magnetism based on coordination compounds has experienced a renaissance in the last 2 decades with the discovery of some molecular complexes that exhibited slow relaxation of the magnetization, i.e., magnetic hysteresis without undergoing three-dimensional (3D) magnetic ordering. These nanomagnets, called single-molecule magnets (SMMs),[1] straddle the quantum/classical interface showing quantum effects such as quantum tunneling of the magnetization and quantum phase interference. They are also potential candidates for magnetic information storage and quantum computing.[2] More recently, the discovery of a similar magnetic behavior in one-dimensional (1D) systems has expanded the field of nanomagnets. These latter systems, named single-chain magnets (SCMs),[3] are able to exhibit magnetic hysteresis at higher temperatures than SMMs and, therefore, are promising materials for the achievement of future devices for magnetic information storage and processing at more accessible and cost-efficient temperatures. Two requirements are needed to observe SCM behavior: first, high Ising-type anisotropy of the magnetic centers or units composing the chain and, second, strong intrachain interactions with very weak interchain interactions to avoid 3D magnetic ordering. Intrachain interactions may be ferro- or antiferromagnetic in nature as long as an overall nonzero magnetization is expected for the chain. The former gives rise to ferromagnetic-type SCMs[4] and the latter to either ferrimagnetic[5] or spin-canted antiferromagnetic SCMs.[6] In some cases, SCM behavior is observed when anisotropic high-spin units, such as $S_T = 4Mn_2^{III}$ dinuclear units,[3] antiferromagnetically coupled

*To whom correspondence should be addressed. E-mail: ecolacio@ugr.es (E.C.), clerac@crpp-bordeaux.cnrs.fr (R.C.).

(1) For some recent reviews, see: Christou, G.; Gatteschi, D.; Hendrickson, D. N.; Sessoli, R. *MRS Bull.* **2000**, *25*, 66. Gatteschi, D.; Sessoli, R. *Angew. Chem., Int. Ed.* **2003**, *42*, 268. Christou, G. *Polyhedron* **2005**, *24*, 2065. Gatteschi, D.; Sessoli, R.; Villain, J. *Molecular Nanomagnets*; Oxford University Press: Oxford, U.K., 2006.Aromí, G.; Brechin, E. K. *Struct. Bonding* (*Berlin*) **2006**, *122*, 1. Rebilly, J.-N.; Mallah, T. *Struct. Bonding* (*Berlin*) **2006**, *122*, 103. Cornia, A.; Costantino, A. F.; Zobbi, L.; Caneschi, A.; Gatteschi, D.; Mannini, M.; Sessoli, R. *Struct. Bonding* (*Berlin*) **2006**, *122*, 133. Milios, C. J.; Piligkos, S.; Brechin, E. K. *Dalton Trans.* **2008**, 1809. Andruh, M.; Costes, J.-P.; Diaz, C.; Gao, S. *Inorg. Chem.* **2009**, *48*, 3342.

(2) (a) Wernsdorfer, W.; Sessoli, R. *Science* **1999**, *284*, 133. (b) Leuenberger, M. N.; Loss, D. *Nature* **2001**, *410*, 789. (c) Meier, F.; Loss, D. *Physica B* **2003**, *329*, 1140.

(3) For some recent reviews, see: Coulon, C.; Miyasaka, H.; Clérac, R. *Struct. Bonding* (*Berlin*) **2006**, *122*, 163. Miyasaka, H.; Julve, M.; Yamashita, M.; Clérac, R. *Inorg. Chem.* **2009**, *48*, 3420.

(4) Lescouëzec, R.; Toma, L. M.; Vaissermann, J.; Verdaguer, M.; Delgado, F. S.; Ruiz-Pérez, C.; Lloret, F.; Julve, M. *Coord. Chem. Rev.* **2005**, *249*, 2691. Toma, L. M.; Lescouëzec, R.; Pasan, J.; Ruiz-Pérez, C.; Vaissermann, J.; Cano, J.; Carrasco, R.; Wernsdorfer, W.; Lloret, F.; Julve, M. *J. Am. Chem. Soc.* **2006**, *128*, 4842.

(5) Pardo, E.; Ruiz-García, R.; Lloret, F.; Faus, J.; Julve, M.; Journaux, Y.; Delgado, F.; Ruiz-Pérez, C. *Adv. Mater.* **2004**, *16*, 1597.

(6) Palii, A. V.; Ostrovski, S. M.; Klokishner, S. I.; Reu, O. S.; Su, Z.-M.; Prosvirin, A. V.; Zhao, H.-H.; Mao, J.-G.; Dunbar, K. R. *J. Phys. Chem. A* **2006**, *110*, 14003. Bernot, K.; Luzon, J.; Sessoli, R.; Vindigni, A.; Thion, J.; Richeter, S.; Leclerq, D.; Larionova, J.; van der Lee, A. *J. Am. Chem. Soc.* **2008**, *130*, 1619. Yoon, J. H.; Ryu, D. W.; Kim, H. C.; Yoon, S. W.; Suh, B. J.; Hong, C. S. *Chem.—Eur. J.* **2009**, *15*, 3661.

 Published on Web 01/15/2010

$Mn^{III}-Ni^{II}-Mn^{III}$ units,[3] or SMM systems,[7] are ferromagnetically coupled along the chain. In the past few years, much effort has been devoted to the rational preparation of SCM systems, but only a limited number of these have been structurally and magnetically characterized. The early SCMs were made from 3d,[6,8] 3d-radical,[9] 3d−3d,[4,5,10] and 3d−5d[11] spin carriers. Unfortunately, these systems exhibited magnetic hysteresis at too low temperature for practical applications. In view of this, Ln^{III} cations with large magnetic anisotropy were further assembled with radical or metal complexes with the aim of obtaining 4f-radical[12] and 3d−4f[13] chain systems that could eventually behave as SCMs at higher temperatures. Although some achievements have been reached in this direction, more examples of 1D systems with different bridging ligands and couples of 3d−4f metal ions still need to be studied. In this context, we report here the synthesis, crystal structures, and magnetic properties of a family of 1D $Ni^{II}_2Ln^{III}$ cationic complexes of formulas $\{[Ni_2(mbpb)_3]Tb(H_2O)_5\}(NO_3)\cdot 3THF\cdot 7H_2O$ (**1**) and $\{[Ni_2(mbpb)_3]Ln(H_2O)_6\}(CF_3SO_3)\cdot 7H_2O$ (Ln = Tb, **2**; Dy, **3**; Gd, **4**). Tb^{3+} and Dy^{3+} have been chosen because they possess intrinsic high-spin and strong Ising-type anisotropy and therefore satisfy one of the requirements needed to observe slow relaxation of the magnetization. This, together with the anisotropy of the Ni^{II} ions, which is due to zero-field-splitting effects, might favor SCM behavior of **1**−**3**. Conversely, Gd^{III} has been chosen because of its isotropic nature, and therefore the $Ni^{II}-Gd^{III}$ magnetic exchange interaction can be easily determined in **4**.

Experimental Section

General Procedures. All analytical reagents were purchased from commercial sources and used without further purification. The 1,3-bis(pyridine-2-carboxamide)benzene (H_2mbpb) ligand was prepared according to a previously described procedure.[14]

Preparation of the Complexes. $\{[Ni_2(mbpb)_3]Tb(H_2O)_5\}(NO_3)\cdot 3THF\cdot 7H_2O$ **(1).** A solution of NaOH (0.2 g, 5 mmol) in 10 mL of water and a solution of $Ni(NO_3)_2\cdot 6H_2O$ (0.485 g, 1.67 mmol) in 5 mL of water were successively added dropwise to a suspension of the H_2mbpb ligand (0.795 g, 2.5 mmol) in 25 mL of water, and the mixture was refluxed for 2 h (solution A). Slow diffusion of a water solution (3 mL) of $Tb(NO)_3\cdot 6H_2O$ (0.170 g, 0.375 mmol) into 3 mL of solution A (0.083 mmol) through a 3 mL tetrahydrofuran (THF) layer in a 2.5-cm-diameter glass tube afforded after 2 weeks green crystals of **1**. Yield: 32%. Anal. Calcd for $C_{66}H_{84}N_{13}O_{24}Ni_2Tb$: C, 46.09; H, 4.92; N, 10.59. Found: C, 46.01; H, 4.60; N, 10.54. IR (KBr, cm^{-1}): 3393, ν(OH); 1610, ν(C═O); 1581, ν(C═C); 1561, ν(CN); 1384, $\nu(NO_3)$.

$\{[Ni_2(mbpb)_3]Tb(H_2O)_6\}(CF_3SO_3)\cdot 7H_2O$ **(2).** A solution of $Tb(CF_3SO_3)_3$ (0.076 g, 0.125 mmol) in 5 mL of water was added to 6 mL of solution A (0.125 mmol). A light-green precipitate immediately formed. The mixture was stirred for 30 min. After filtration of the light-green solid, the resulting green solution was allowed to stand at room temperature. X-ray-quality light-green crystals of **2** were obtained by slow evaporation of the solution after several days. They were filtered off and air-dried. Yield: 53%. Anal. Calcd for $C_{55}H_{62}N_{12}O_{22}Ni_2TbSF_3$: C, 41.07; H, 3.89; N, 10.45. Found: C, 41.19; H, 4.22; N, 10.28. IR (KBr, cm^{-1}): 3371, ν(OH); 1610, ν(C═O); 1582, ν(C═C); 1559, ν(CN); 1276, 1261, $\nu(CF_3SO_3)$.

$\{[Ni_2(mbpb)_3]Dy(H_2O)_6\}(CF_3SO_3)\cdot 7H_2O$ **(3).** This compound was synthesized by following the same procedure as that for **2** but using $Dy(CF_3SO_3)_3$ (0.076 g, 0.125 mmol). The resulting light-green solution was kept at room temperature, and X-ray-quality light-green crystals of **3** were obtained by slow evaporation of the solution after several days. They were filtered off and air-dried. Yield: 48%. Anal. Calcd for $C_{55}H_{62}N_{12}O_{22}Ni_2DySF_3$: C, 40.98; H, 3.88; N, 10.43. Found: C, 40.52; H, 4.01; N, 10.53. IR (KBr, cm^{-1}): 3370, ν(OH); 1610, ν(C═O); 1581, ν(C═C); 1560, ν(CN); 1273, 1259, $\nu(CF_3SO_3)$.

$\{[Ni_2(mbpb)_3]Gd(H_2O)_6\}(CF_3SO_3)\cdot 7H_2O$ **(4).** This compound was synthesized by following the same procedure as that for **2** but using $Gd(CF_3SO_3)_3$ (0.076 g, 0.125 mmol). In this case, a microcrystalline green powder was obtained by evaporation of the green solution. Yield: 69%. Anal. Calcd for $C_{55}H_{62}N_{12}O_{22}Ni_2GdSF_3$: C, 41.11; H, 3.89; N, 10.46. Found: C, 40.77; H, 4.21; N, 10.33. IR (KBr, cm^{-1}): 3392, ν(OH); 1611, ν(C═O); 1581, ν(C═C); 1559, ν(CN); 1277, 1259, $\nu(CF_3SO_3)$.

Physical Measurements. Elemental analyses were carried out at the "Centro de Instrumentación Cientifica" (University of Granada) on a Fisons-Carlo Erba analyzer model EA 1108. The IR spectra on powdered samples were recorded with a Thermo-Nicolet IR200FTIR by using KBr pellets. The magnetic susceptibility measurements were obtained with the use of a Quantum Design SQUID magnetometer MPMS-XL operating at different magnetic fields up to 7 T and between 1.9 and 300 K. Measurements were performed on polycrystalline samples. Alternating-current (ac) susceptibility measurements have been measured with an oscillating ac field of 3 Oe and ac frequencies ranging from 1 to 1500 Hz. The magnetic data were corrected for the sample holder and the diamagnetic contributions.

Single-Crystal Structure Determination. Suitable crystals of **1**−**3** were mounted on glass fibers and used for data collection. Data were collected with a Bruker APEX CCD (**2**) or Bruker X8 Proteum (**1** and **3**) diffractometer at 150(2) K. The data were processed with *APEX2*[15] and corrected for absorption using *SADABS*.[16] The structures were solved by direct methods using *SIR97*,[17] revealing positions of all non-hydrogen atoms. These atoms were refined on F^2 by a full-matrix least-squares procedure using anisotropic displacement parameters.[18] All hydrogen

(7) Lecren, L.; Wernsdorfer, W.; Li, Y.-G.; Vindigni, A.; Miyasaka, H.; Clérac, R. *J. Am. Chem. Soc.* **2007**, *129*, 5045. Xu, H.-B.; Wang, B.-W.; Pan, F.; Wang, Z.-M.; Gao, S. *Angew. Chem., Int. Ed.* **2007**, *46*, 7388. Ferbinteanu, M.; Miyasaka, H.; Wernsdorfer, W.; Nakata, K.; Sugiura, K.; Yamashita, M.; Coulon, C.; Clérac, R. *J. Am. Chem. Soc.* **2005**, *127*, 3090.

(8) Zheng, Y.-Z.; Xue, W.; Tong, M.-L.; Chen, X.-M.; Zheng, S.-L. *Inorg. Chem.* **2008**, *47*, 11202. Gavrilenko, K. S.; Cador, O.; Bernot, K.; Rosa, P.; Sessoli, R.; Golhen, S.; Pavlishchuck, V. V.; Ouahab, L. *Chem.—Eur. J.* **2008**, *14*, 2034.

(9) Caneschi, A.; Gatteschi, D.; Lalioti, N.; Sangregorio, C.; Sessoli, R.; Venturi, G.; Vindigni, A.; Rettori, A.; Pini, M. G.; Novak, M. A. *Angew. Chem., Int. Ed.* **2001**, *40*, 1760. Miyasaka, H.; Mandanbashi, T.; Sugimoto, K.; Nakazawa, Y.; Wernsdorfer, W.; Sugiura, K.-I.; Yamashita, M.; Coulon, C.; Clérac, R. *Chem.—Eur. J.* **2006**, *12*, 7028.

(10) Clérac, R.; Miyasaka, H.; Yamashita, M.; Coulon, C. *J. Am. Chem. Soc.* **2002**, *124*, 12837. Miyasaka, H.; Clérac, R.; Mizushima, K.; Sugiura, K.; Yamashita, M.; Wernsdorfer, W.; Coulon, C. *Inorg. Chem.* **2003**, *42*, 8203. Miyasaka, H.; Saitoh, A.; Yamashita, M.; Clérac, R. *Dalton Trans.* **2008**, 2422.

(11) Choi, S. W.; Kwak, H. Y.; Yoon, J. H.; Kim, H. C.; Koh, E. K.; Hong, C. S. *Inorg. Chem.* **2008**, *47*, 10214.

(12) Bogani, L.; Sangregorio, C.; Sessoli, R.; Gatteschi, D. *Angew. Chem., Int. Ed.* **2005**, *44*, 5817. Bernot, K.; Bogani, L.; Caneschi, A.; Gatteschi, D.; Sessoli, R. *J. Am. Chem. Soc.* **2006**, *128*, 7947.

(13) Costes, J.-P.; Clemente-Juan, J. M.; Dahan, F.; Milon, J. *Inorg. Chem.* **2004**, *43*, 8200. Huang, Y. G.; Wang, X.-T.; Jiang, F. L.; Gao, S.; Wu, M.-Y.; Gao, Q.; Wei, W.; Hong, M. C. *Chem.—Eur. J.* **2008**, *14*, 10340.

(14) Dutta, S.; Bhattacharya, P. K. *J. Chem. Res.* **2000**, 362.

(15) *Bruker Apex2*; Bruker AXS Inc.: Madison, WI, **2004**.

(16) Sheldrick, G. M. *SADABS, Program for empirical adsorption correction*; Institute for Inorganic Chemistry, University of Göttingen: Göttingen, Germany, **1996**.

(17) Altomare, A.; Burla, M. C.; Camilla, M.; Cascarano, G. L.; Giacovazzo, C.; Guagliardi, A.; Moliterni, A. G. G.; Polidori, G.; Spagna, R. *J. Appl. Crystallogr.* **1999**, *32*, 115.

(18) Sheldrick, G. M. *SHELX 97, Program for crystal structure refinement*; University of Göttingen: Göttingen, Germany, **1997**.

Table 1. Crystallographic Data and Structural Refinement Details for Compounds **1**−**3**

	1	**2**	**3**
chemical formula	$C_{66}H_{36}N_{13}O_{24}Ni_2Tb$	$C_{55}H_{36}N_{12}O_{21}F_3SNi_2Tb$	$C_{55}H_{36}N_{12}O_{21}F_3SNi_2Dy$
M (g mol^{-1})	1671.42	1566.36	1569.94
T (K)	150	150	150
λ (Å)	0.710 69	1.541 78	1.541 78
cryst syst	monoclinic	monoclinic	monoclinic
space group	$P2_1/n$	$P2_1/c$	$P2_1/c$
a (Å)	10.744(5)	12.8938(7)	12.9029(7)
b (Å)	35.592(5)	16.8784(10)	16.9341(10)
c (Å)	19.347(5)	28.5936(17)	28.3232(17)
α (deg)	90	90	90
β (deg)	101.159(5)	90.860(3)	90.288(3)
γ (deg)	90	90	90
V (Å^3)	7258(4)	6222(6)	6188.5(6)
Z	4	4	4
ρ (g cm^{-3})	1.530	1.672	1.685
μ (mm^{-1})	1.563	7.336	8.216
no. of unique reflns	52 055	87 751	38 557
R(int)	0.049	0.087	0.317
GOF on F^2	1.277	1.045	0.747
R1[a] [$I > 2\sigma(I)$]	0.080	0.047	0.102
wR2[a] [$I > 2\sigma(I)$]	0.177	0.125	0.223

[a] $R1(F) = \sum||F_o| - |F_c||/\sum|F_o|$; $wR2(F^2) = [\sum w(F_o^2 - F_c^2)^2/\sum wF^4]^{1/2}$.

atoms were located in difference Fourier maps and included as fixed contributions riding on attached atoms with isotropic thermal displacement parameters 1.2 times those of the respective atom. Final R1(F), wR2(F^2), goodness-of-fit agreement factors, and details of the data collection and analyses for **1** and **2** can be found in Table 1. It should be noted that crystals of **3** undergo a very fast degradation when removed from the mother liquor, which has a high impact on the quality of the data. Several crystals of **3** were measured, and the structure was solved from the best data that we were able to collect. Crystallographic and structure refinement data are given in Table 1. We have chosen to include the CIF file for **3** as Supporting Information but not to deposit them in the CCDC crystallographic database. CCDC reference numbers are 750064 (**1**) and 750065 (**2**).

XRPD Analysis of 4. The powders were gently ground in an agate mortar and then deposited with care in the hollow of an aluminum holder equipped with a zero-background plate. Diffraction data (Cu Kα, λ = 1.5418 Å) were collected on a θ:θ Bruker AXS D8 vertical scan diffractometer equipped with primary and secondary Soller slits, a secondary-beam curved graphite monochromator, a Na(Tl)I scintillation detector, and pulse height amplifier discrimination. The generator was operated at 40 kV and 40 mA. Optics used are the following: divergence 0.5°, antiscatter 0.5°, receiving 0.2 mm. Indexing was obtained with the aid of *TREOR*[19] [monoclinic, a = 12.887 Å, b = 16.967 Å, c = 28.231 Å, and β = 91.201°]. Systematic absences indicated $P2_1/c$ as the probable space group, later confirmed by a successful solution and refinement by using the technique implemented in *Topas-R*.[20]

Results and Discussion

The 1D Ni_2Ln systems were prepared by following the strategy of "complexes as ligands". We have recently reported the bis-bidentate dinucleating bridging ligand H_2mbpb, which contains a *m*-phenylene linker. This ligand is able to afford anionic triple-stranded dinickel(II) mesocates of formula $[Ni_2(mbpb)_3]^{2-}$ that exhibit ferromagnetic coupling of about $J_{Ni-Ni} = +3.6$ cm^{-1} (with the following spin Hamiltonian definition: $H = -J_{Ni-Ni}\, S_{Ni1}S_{Ni2}$) between the Ni^{II} ions through the bridging ligand by the spin-polarization mechanism.[21] This anionic unit (see Scheme 1) possesses oxygen donor atoms belonging to the coordinated carboxamide groups of the fully deprotonated $mbpb^{2-}$ ligands and, in principle, could be used as the ligand to coordinate oxophilic Ln^{III} ions.

Thus, the assembly of the in situ generated dinuclear $[Ni_2(mbpb)_3]^{2-}$ building block with either $Tb(NO_3)_3\cdot 6H_2O$ or $Ln(CF_3SO_3)_3$ (Ln = Gd^{3+}, Tb^{3+}, Dy^{3+}) afforded the 3d−3d−4f carboxamidate-bridged 1D complexes of formulas $\{[Ni_2(mbpb)_3]Tb(H_2O)_5\}(NO_3)\cdot 3THF\cdot 7H_2O$ (**1**) and $\{[Ni_2(mbpb)_3]Ln(H_2O)_6\}(CF_3SO_3)\cdot 7H_2O$ (Ln = Tb, **2**; Dy, **3**; Gd, **4**).

The structure of **1** is made of 1D cationic chains $\{[Ni_2(mbpb)_3]Tb(H_2O)_5\}^+$ (Figure 1) extended along the (101) direction, one nitrate anion, three THF molecules, and seven crystallization water molecules, which are all involved in an extensive network of hydrogen bonds.

Within the chains, Tb^{3+} are connected by $[Ni_2(mbpb)_3]^{2-}$ metalloligand units, which act as bidentade/bridging ligands. In this coordination mode, each $[Ni_2(mbpb)_3]^{2-}$ unit is connected to two Tb^{III} ions through two amidate oxygen atoms of two different $mbpb^{2-}$ strands, with O−Tb distances of 2.269 and 2.196 Å (Figure 2). One of these oxygen atoms is located in the upper part of the $[Ni_2(mbpb)_3]^{2-}$ unit and the other one in the lower part. Because two neighboring $[Ni_2(mbpb)_3]^{2-}$ units of the chain coordinate the Tb^{3+} ion through the amidate oxygen atoms of the same part (upper or lower), the Tb^{3+} ions exhibit a zigzag conformation along the chain with a Tb−Tb−Tb angle of 120°.

The coordination sphere around the Tb^{III} ions is completed by five water molecules, leading to a TbO_7 coordination environment with Tb−Ow distances varying between 2.335 and 2.391 Å. The degree of distortion of the Tb coordination polyhedron with respect to ideal seven-vertex polyhedra was quantified by the continuous shape measure theory.[22] By using the *SHAPE* software,[23] we compute the shape measure relative to the pentagonal bipyramid (D_{5h}), capped trigonal prism (C_{2v}), and capped octahedron (C_{3v}) with values of 1.16, 2.78, and 4.23, respectively. The shape measures relative to other reference polyhedra are significantly larger. Therefore, the TbO_7 coordination sphere is clearly a pentagonal bipyramid. In this description, the two carboxamide oxygen atoms occupy axial and equatorial positions and therefore adopt a cis disposition. The O−Tb−O angles in the equatorial plane fall into the 69.69−76.76° range, whereas the axial O−Tb−O angle is 173.08°. On the other hand, the structural parameters of the distorted Ni_2 dinuclear unit show no significant differences from those observed in the heteronuclear complex $\{Ag_2(H_2O)[Ni_2(mbpb)_3]\}\cdot 11H_2O$.[21] The Tb···Tb, Ni···Ni, and two Tb···Ni distances within the chain are 10.257, 6.970, 6.322, and 6.401 Å, respectively.

(19) Werner, P. E.; Eriksson, L.; Westdahl, M. *J. Appl. Crystallogr.* **1985**, *18*, 367.
(20) *Topas-R, General profile and structure analysis software for powder diffraction data*; Bruker AXS: Karlsruhe, Germany, 2001.
(21) Palacios, M. A.; Rodríguez-Diéguez, A.; Sironi, A.; Herrera, J. M.; Mota, A. J.; Cano, J.; Colacio, E. *Dalton Trans.* **2009**, 8538.
(22) Pinsky, M.; Avnir, D. *Inorg. Chem.* **1998**, *37*, 5575. Casanova, D.; Llunell, M.; Alemany, P.; Alvarez, S. *Chem.—Eur. J.* **2005**, *11*, 1479. Casanova, D.; Alemany, P.; Bofill, J. M.; Alvarez, S. *Chem.—Eur. J.* **2003**, *9*, 1281.
(23) Llunell, M.; Casanova, D.; Cirera, J.; Bofill, J. M.; Alemany, P.; Alvarez, S.; Pinsky, M.; Avnir, D. *SHAPE*, version 1.1b; University of Barcelona: Barcelona, Spain, **2005**.

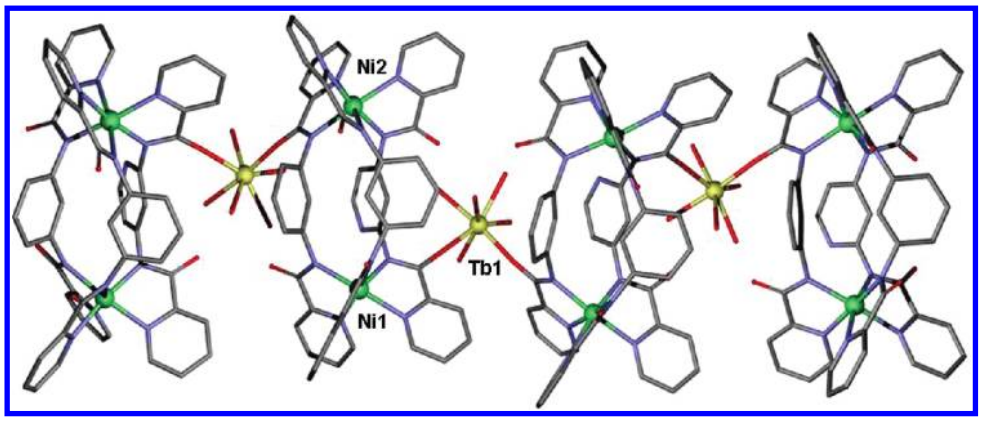

Figure 1. Perspective view of the chain structure of **1**.

Scheme 1. Ligand H_2mbpb and the Anionic Metalloligand $[Ni_2(mbpb)_3]^{2-}$

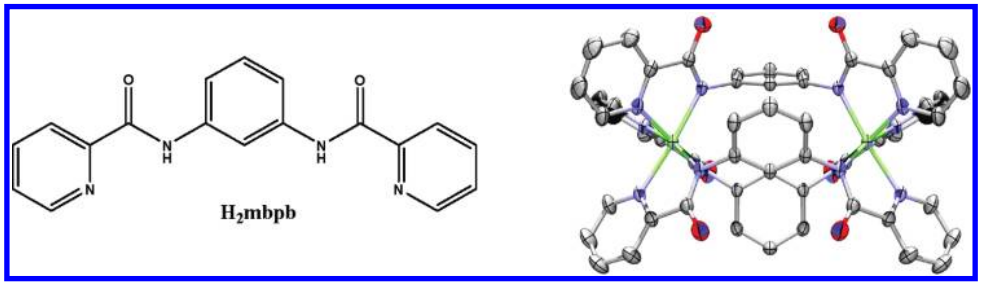

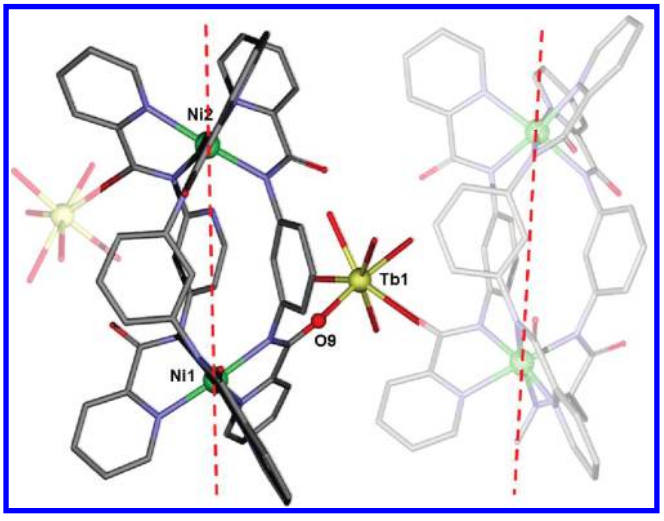

Figure 2. Perspective view of the asymmetric unit of **1**.

At the supramolecular level, the chains are glued by strong hydrogen-bond interactions involving the coordinated water molecules of a chain and the noncoordinated amidate oxygen atoms of neighboring chains, with donor−aceptor O···O distances falling within the 2.599−2.824 Å range. These supramolecular interactions give rise to a two-dimensional (2D) network (Figure 3).

The crystallization water molecules, the THF molecules, and the nitrate anions are involved in hydrogen-bond interactions giving rise to the formation of 2D arrays, which are intercalated between the layers of hydrogen-bonded chains (Figure 4).

Complexes **2** and **3** are isostructural. In the case of compound **3**, the bad quality of the data prevents an accurate resolution of the structure. Nevertheless, the chain part of the structure of **3** can be considered as correct. Because of this, we have chosen to include the CIF file as Supporting Information but not to deposit it in the CCDC crystallographic database. Although we have not succeeded in obtaining suitable crystals of **4** for X-ray crystal structure determination, powder diffraction measurements (see Figure S1 in the Supporting Information) clearly show that **4** is isostructural with **2** and **3**. In view of the above considerations, only the structural data for **2** will be given here.

Although the chain structure of **2** is, in general, similar to that of **1** (see Figure 5), the use of triflate instead of nitrate as the counterion gives rise to some important structural differences: (i) Tb^{3+} cations exhibit a LnO_8 coordination environment with dodecahedral geometry (the shape measure relative to the trigonal dodecahedron is the lowest with a value of 0.79). (ii) The steric crowding around the Tb^{3+} cations for the eight-coordination mode is greater than for the seven-coordination mode observed in **1**. Consequently, the Tb−O bond distances for **2**, which vary between 2.382 and 2.462 Å, are greater than those observed for **1**. The shortest distances correspond to the $Tb-O_{amidate}$ bonds with values of 2.328 and 2.247 Å. (iii) As a consequence of the longer Tb−O distances found in **2**, the Tb···Tb and two Tb···Ni distances within the chain of 10.902, 6.497, and 6.379 Å, respectively, are greater than those observed for **1**. The Ni···Ni distance of 6.970 Å is only slightly shorter than that for **1**. (iv) The lines connecting Ni^{2+} inside the $[Ni_2(mbpb)_3]^{2-}$ dinuclear units (red lines in Figures 2 and 6) are almost parallel in **1** and significantly titled in **2**. (v) Chains propagate along the *b* axis with Tb−Tb−Tb angles rather smaller than that observed in **1** (101.6°). (vi) In **2**, two of the coordinated water molecules are not involved in hydrogen-bond interactions with the amidate oxygen atoms of the

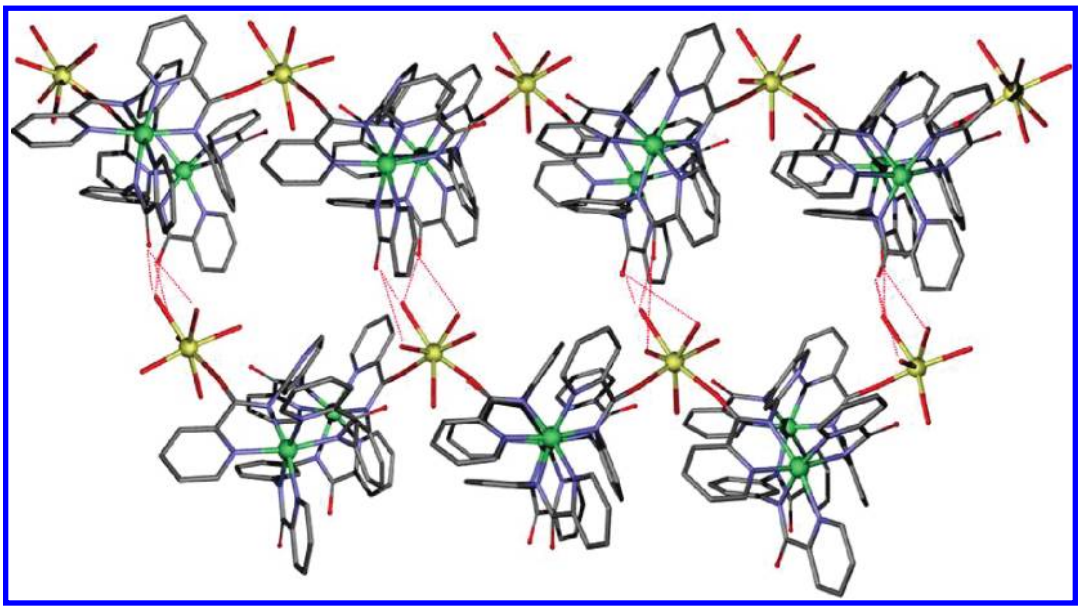

Figure 3. View of the hydrogen-bond interactions (red lines) connecting chains in **1**.

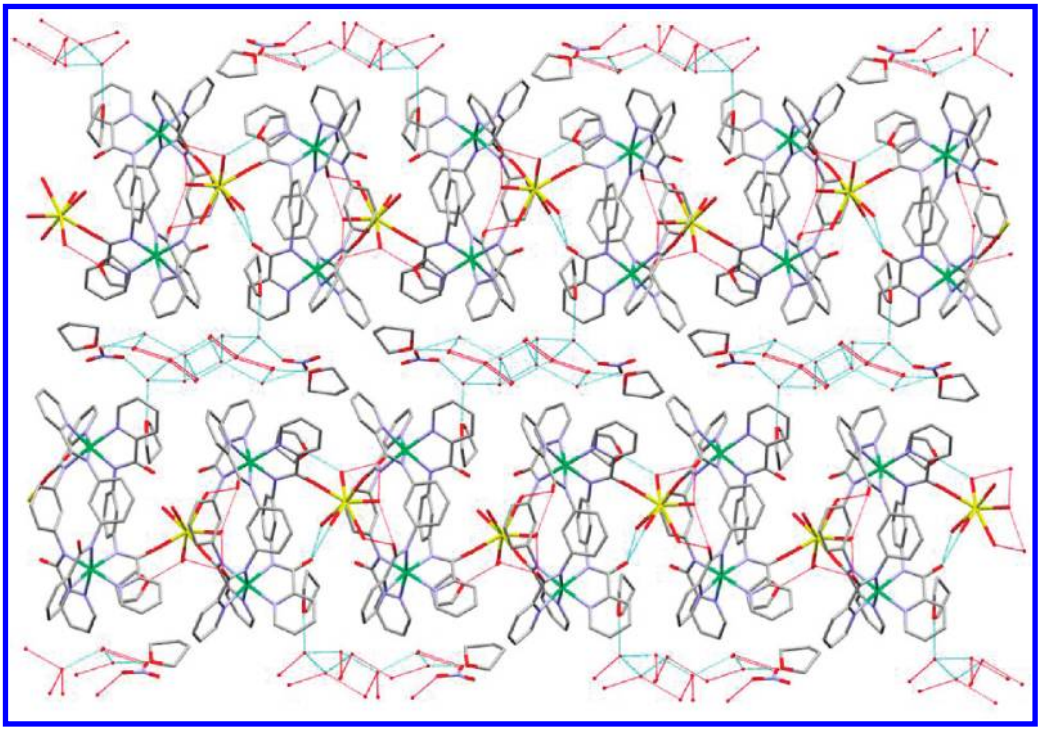

Figure 4. View of the 3D network for **1**.

$[Ni_2(mbpb)_3]^{2-}$ units belonging to neighboring chains. Concretely, one of them forms hydrogen bonds with a crystallization water molecule, whereas the other one interacts with the amidate oxygen atom of the $[Ni_2(mbpb)_3]^{2-}$ unit to which Tb^{3+} is coordinated. The donor−acceptor $Ow\cdots O_{amidate}$ distances are in the 2.706−2.748 Å range. Cationic chains, triflate anions, and crystallization water molecules form a hydrogen-bond 3D network.

Magnetic Properties

The temperature dependence of the $\chi_M T$ product for **1** at 1000 Oe is given in the Figure 7. The room temperature $\chi_M T$ value of 11.1 cm^3 K mol^{-1} is slightly low but still in relatively good agreement with the expected value (13.8 cm^3 K mol^{-1}) for two Ni^{II} metal ions ($S = 1$, $C = 1$ cm^3 K mol^{-1}) and one Tb^{III} metal ion ($S = 3$, $L = 3$, $^7F_6$ $g = {}^3/_2$: $C = 11.815$ cm^3 K mol^{-1}) in the free-ion approximation.[24] The $\chi_M T$ product decreases continuously upon decreasing temperature, first slowly to 50 K and further sharply to reach a value of 7.3 cm^3 K mol^{-1} at 1.83 K. In Ln^{3+} complexes, the interelectronic repulsions and the spin−orbit coupling give rise to $^{2S+1}L_J$ states, which are further split into Stark components by crystal-field effects on the order of 100 cm^{-1}. The number

(24) Benelli, C.; Gatteschi, D. *Chem. Rev.* **2002**, *102*, 2369 and references cited therein. Sutter, J. P.; Kahn, O. *Magnetism: Molecules to Materials*; Miller, J. S., Drillon, M., Eds.; Wiley-VCH: Weinheim, Germany, 2005; Vol. *V*, p 161

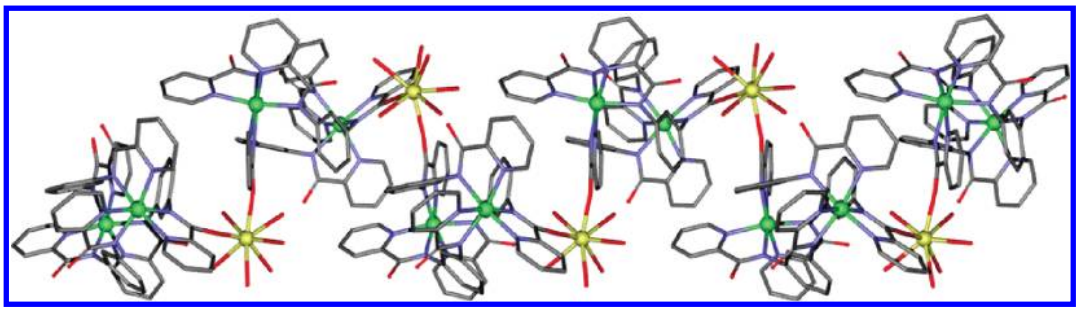

Figure 5. Perspective view of the chain structure of **2**.

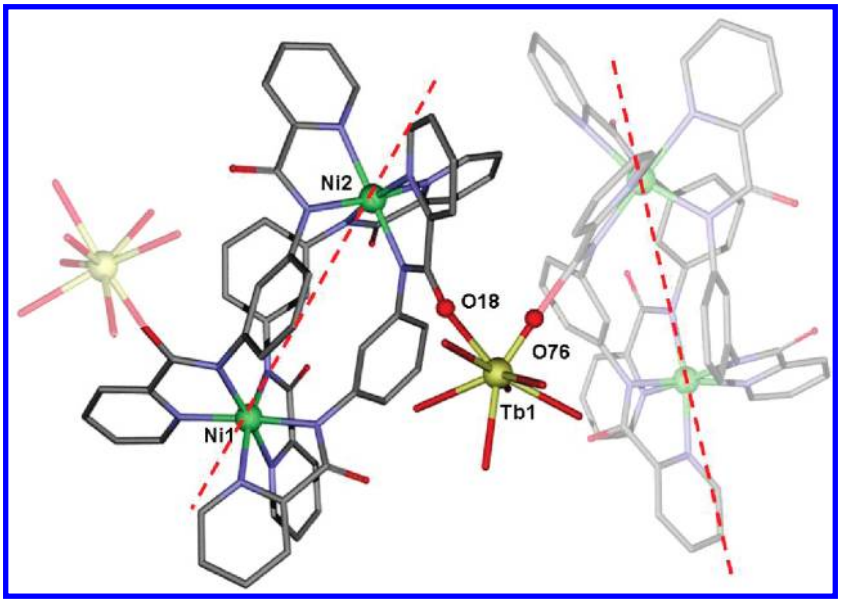

Figure 6. Perspective view of the asymmetric unit of **2**.

of Stark sublevels arising from the ground state depends on the crystal-field symmetry.[24] At room temperature, all of the ground-state Stark sublevels are statistically populated and the free-ion approximation applies. However, when the temperature is lowered, depopulation of these sublevels leads to a deviation of the $\chi_M T$ product from the Curie law.[25] Moreover, because the magnetic exchange constants are expected to be weak for 3d−4f systems,[24,26,27] the decrease of the $\chi_M T$ product in this compound is mainly due to the depopulation of the Stark sublevels and not to the magnetic exchange interactions. This behavior hides the ferromagnetic

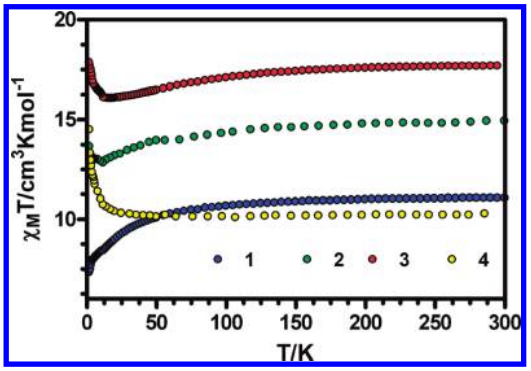

Figure 7. Temperature dependence of the $\chi_M T$ product for **1** (blue dots), **2** (green dots), **3** (red dots), and **4** (yellow dots) at 1000 Oe (with χ_M as the molar susceptibility defined as M/H per Ni_2Ln unit).

Ni−Ni interactions (i.e., the increase of the $\chi_M T$ product) known to be present in the dinuclear $[Ni_2(mbpb)_3]^{2-}$ moiety[21] but also encumbers the determination of the nature of the magnetic exchange interaction between Ni^{2+} and Tb^{3+} ions through the amidato bridging group. The local effects of the Tb^{3+} cation due to depopulation of the Stark sublevels could be evaluated by comparing the magnetic properties of **1** with those of the isostructural compound Zn_2Tb. However, all attempts to obtain this compound failed.

The field dependence of the magnetization below 8 K (Figure 8, inset) reveals a relatively slow increase of the

(25) Kahn, O. *Molecular Magnetism*; VCH: Weinheim, Germany, 1993.
(26) Costes, J.-P.; Dahan, F.; Dupuis, A.; Laurent, J.-P. *Inorg. Chem.* **1997**, *36*, 4284. Costes, J.-P.; Dahan, F.; Dupuis, A.; Laurent, J.-P. *Inorg. Chem.* **2000**, *39*, 165. Fellah, F. Z. C.; Costes, J.-P.; Dahan, F.; Duhayon, C.; Novitchi, G.; Tuchagues, J.-P.; Vendier, L. *Inorg. Chem.* **2008**, *47*, 6444. Pointillart, F.; Bernot, K.; Sessoli, R.; Gatteschi, D. *Chem.—Eur. J.* **2007**, *13*, 1602. Chandrasekhar, V.; Pandian, B. M.; Boomishankar, R.; Steiner, A.; Vittal, J. J.; Houri, A.; Clérac, R. *Inorg. Chem.* **2008**, *47*, 4918. Mori, F.; Ishida, T.; Nogami, T. *Polyhedron* **2005**, *24*, 2588. Yamaguchi, T.; Sunatsuki, Y.; Ishida, H.; Kojima, M.; Akashi, H.; Re, N.; Matsumoto, N.; Pochaba, A.; Mrozinski, J. *Inorg. Chem.* **2008**, *47*, 5736. Shiga, T.; Ito, N.; Hidaka, A.; Ohkawa, H.; Kitagawa, S.; Ohba, M. *Inorg. Chem.* **2007**, *46*, 3492. Barta, C. A.; Bayly, S. R.; Read, P. W.; Patrick, B. O.; Thompson, R. C.; Orvig, C. *Inorg. Chem.* **2008**, *47*, 2280. Dhers, S.; Sahoo, S.; Costes, J.-P.; Duhayon, C.; Ramasesha, S.; Sutter, J.-P. *CrystEngComm* **2009**, *11*, 2078. Sutter, J.-P.; Dhers, S.; Rajamani, R.; Ramasesha, S.; Costes, J.-P.; Duhayon, C.; Vendier, L. *Inorg. Chem.* **2009**, *48*, 5820. Costes, J.-P.; Yamaguchi, T.; Kojima, M.; Vendier, L. *Inorg. Chem.* **2009**, *48*, 5555.
(27) Madalan, A. M.; Bernot, K.; Pointillart, F.; Andruh, M.; Caneschi, A. *Eur. J. Inorg. Chem.* **2007**, 5533.

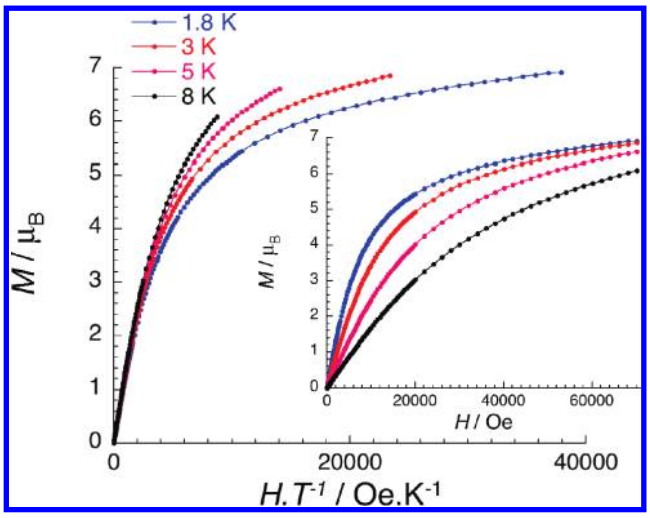

Figure 8. M vs H/T and M vs H (inset) plots for **2**.

magnetization at low fields and then a linear increase without clear saturation above 4 T. The magnetization at 1.8 K and 7 T is 7.32 μ_B. The linear high-field variation of the magnetization suggests the presence of a significant magnetic anisotropy and also likely low-lying excited states that are partially thermally and field-induced populated. These low-lying excited states are in agreement with weak magnetic interactions along the Ni_2Tb chain. These two features can also be highlighted by plotting M versus H/T at different fields (Figure 8); i.e., the curves are not all superposed on a single master curve like for isotropic systems. The important magnetic anisotropy observed for **1** may be the main reason for which the room temperature $\chi_M T$ value is not close to that predicted in the free-ion approximation.

The thermal variation of the $\chi_M T$ product for **2** at 1000 Oe is given in Figure 7. The value at 300 K (14.9 cm^3 K mol^{-1}) is not far from that expected, 13.8 cm^3 K mol^{-1}, especially considering than Ni^{II} g values are usually higher than 2. The $\chi_M T$ product decreases continuously with decreasing temperature to reach a minimum at 12.8 K and then shows a sharp increase down to 2 K to a value of 13.6 cm^3 K mol^{-1}. It seems that the effect of depopulation of the Stark sublevels in **2** is not as pronounced as in **1**. This may be due to the fact that, as indicated above, the Tb^{3+} cations in **2** exhibit eight-coordination with Tb−O bond distances longer than those observed for **1**. Such features of the coordination environment give rise to a reduction of the ligand-field effects and therefore to a smaller multiplet width of the Stark sublevels. The field dependence of the magnetization below 8 K is similar to that of **1**, with a value of 8.80 μ_B at 2 K and 5 T. Moreover, the M vs H/T plot (see Figure S2 in the Supporting Information) shows that the magnetic anisotropy is rather significant but smaller than in the case of **1**, thus supporting the reduction of the multiplet width in **2**. The increase of the $\chi_M T$ product at low temperature may be due to the known ferromagnetic interaction between the Ni^{2+} ion in the dinuclear $[Ni_2(mbpb)_3]^{2-}$ unit[21] plus either (i) a ferrimagnetic arrangement of the spin carriers promoted by an antiferromagnetic interaction between Ni^{2+} and Tb^{3+} or (ii) a ferromagnetic interaction between Ni^{2+} and Tb^{3+}. Therefore, the magnetic exchange interaction between Ni^{2+} and Tb^{3+} may not be deduced unambiguously from only the shape of the $\chi_M T$ vs T curve. The isostructural Zn_2Tb compound may permit one to have some qualitative insight into

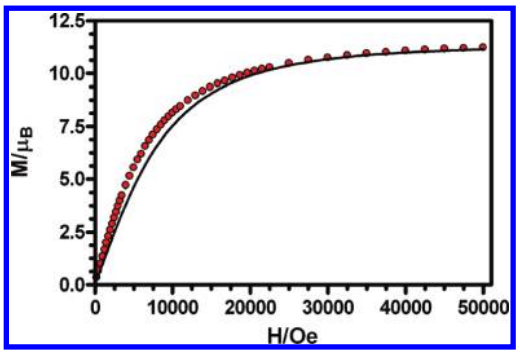

Figure 9. M vs H plot at 2 K for **4**. The solid line is the calculated Brillouin function for an $S = 2$ Ni^{2+} dimer and one isolated Gd^{3+} monomer with $g_{av} = 2.04$.

the nature of the interaction, but, unfortunately, we were not able to obtain such a compound.

At room temperature, the $\chi_M T$ product for **3** of 17.7 cm^3 K mol^{-1} (Figure 7) is in relatively good agreement with the expected value (16.17 cm^3 K mol^{-1}) for two Ni^{II} metal ions ($S = 1$, $C = 1$ cm^3 K mol^{-1} for $g = 2$) and one Dy^{III} metal ion ($S = 5/2$, $L = 5$, $^6H_{15/2}$ $g = {}^4/_3$: $C = 14.17$ cm^3 K mol^{-1}). When the temperature is lowered, the $\chi_M T$ product at 1000 Oe slowly decreases, reaching a value of 16.0 cm^3 K mol^{-1} at 17 K before increasing up to 17.9 cm^3 K mol^{-1} at 1.8 K. The increase from the minimum down to 1.8 K of 1.9 cm^3 K mol^{-1} is greater than that caused by the intradinuclear Ni^{2+}−Ni^{2+} magnetic exchange interaction in the similar chain complex $\{Ag_2(H_2O)[Ni_2(mbpb)_3]\}\cdot 11H_2O$.[21] Unfortunately, this fact does not help to discriminate between the existence of either a ferrimagnetic arrangement of the spin carriers (antiferromagnetic Ni···Dy interaction) or a ferromagnetic interaction between them. The field dependence of the magnetization below 8 K is similar to that of **1** and **2** with a value of 9.7 μ_B at 11.8 K and 7 T. As in **2**, the M vs H/T plot (see Figure S3 in the Supporting Information) shows that the magnetic anisotropy is also smaller than that observed for **1**.

The temperature dependence of χ_MT for **4** at a 1000 Oe magnetic field is shown in Figure 6. The $\chi_M T$ value for **4** at room temperature is 10.3 cm^3 K mol^{-1}, which compares well with the expected value of 9.875 cm^3 K mol^{-1} for two Ni^{2+} and one Gd^{3+} noninteracting metal ions ($S_{Gd} = {}^7/_2$, $S_{Ni} = 1$, $g_{Gd} = 2.0$, $g_{Ni} = 2.0$), especially considering that the average g value might be slightly higher than 2 (i.e., 2.04). This value remains almost constant down to 50 K and below this temperature starts to increase to reach a value of 14.5 cm^3 K mol^{-1} at 2 K. This behavior is consistent with the presence of a weak ferromagnetic interaction between Ni^{2+} and Gd^{3+}, leading to a value at 2 K much higher than that expected for a simple sum of an $S = 2$ Ni^{II} dinuclear complex (3 cm^3 K mol^{-1}) and an $S = {}^7/_2$ Gd^{III} Curie behavior (7.875 cm^3 K mol^{-1}). The dominating ferromagnetic exchange interactions are confirmed by the positive Weiss constant $\theta = 21.4$ K obtained from a Curie−Weiss fit. The value of the magnetization at 5 T of 11.2 μ_B is close to the expected saturation value of 11 μ_B for one Gd^{3+} and two Ni^{2+} ions with $g = 2.0$. The calculated magnetization obtained from the sum of the Brillouin functions for an $S = 2$ Ni^{2+} dimer and one isolated Gd^{3+} with $g_{av} = 2.04$ (note that this value has been fixed to match the experimental data with the theory above 4 T) is below the experimental magnetization (Figure 9), thus supporting the ferromagnetic interaction between Ni^{II} and Gd^{III}.

In spite of the isotropic nature of the Gd^{III} ions, J_{NiNi} and J_{NiGd} could not be extracted because there is no theoretical model available for these types of 1D systems. Previous investigations on isostructural $Ni^{2+}-Ln^{3+}$ complexes have shown that Gd^{III}, Tb^{III}, and Dy^{III} compounds display magnetic exchange interactions of the same nature (generally ferromagnetic).[24,26,27] Therefore, it is reasonable to assume that Ln^{3+} and Ni^{2+} are also weakly ferromagnetically coupled in compounds **1**−**4**, as concluded by Madalan et al. on amidato-bridged Ni−Ln chain compounds.[27]

As indicated above, Tb^{3+} and Dy^{3+} are highly anisotropic ions, and therefore compounds **1**−**3** are good candidates for displaying slow relaxation of the magnetization and, consequently, SCM behavior. The significant θ value for **4** suggests also the existence of a significant ferromagnetic intrachain interaction for compounds **1**−**3**, which would favor the SCM behavior. Because of this, we have performed an ac study on compounds **1**−**3**. However, the ac susceptibility in a zero direct-current field shows the complete absence of an out-of-phase component above 1.8 K. The lack of SCM behavior may be mainly due to the weakness of the intrachain magnetic interactions in **1**−**3**, which does not allow the establishment of a large 1D correlation length above 1.8 K.

Conclusions

The use of the in situ generated dinuclear anionic $[Ni_2(mbpb)_3]^{2-}$ unit as a "ligand" for Ln^{3+} cations (Tb, Dy, Gd) allows the preparation of the first examples of $Ni^{II}_2Ln^{III}$ cationic 1D chains. It is worth noting that the Ln^{3+} coordination number seems to depend on the counteranion present in the structure. Thus, in compound **1**, containing a nitrate anion, the Tb^{3+} ions are seven-coordinated and exhibit a trigonal-bypyramidal geometry. However, in compounds **2**−**4**, containing triflate as the counterion, the Ln^{3+} ions are eight-coordinated and have a geometry that is intermediate between a square antiprism and a dodecahedron. The crystal-field potentials for these two site symmetries are quite different, which has a direct influence on the depopulation of the Stark sublevels, the magnetic anisotropy, and the magnetic properties. Despite the large anisotropy of the Tb^{3+} and Dy^{3+} ions and the existence of a relevant ferromagnetic interaction along the 3d−3d−4f chains, these compounds do not exhibit magnetic slow relaxation and, consequently, SCM behavior. This is mainly due to the weakness of the intrachain magnetic interactions, which hampers the apparition of SCM behavior.

Acknowledgment. This work was supported by the MEC (Spain; Project CTQ-2008-02269/BQU), the Junta de Andalucía (Grant FQM-195), and the Universidad de Granada (grants to A.R.-D., A.J.M., and J.M.H.). M.A. P. thanks the Spanish Ministry of Science and Innovation for a Ph.D. grant. R.C. thanks the European network MAGMANet (Grant NMP3-CT-2005-515767), the University of Bordeaux, the CNRS, the ANR, the GIS Advanced Materials in Aquitaine (COMET Project), and the Région Aquitaine for financial support.

Supporting Information Available: X-ray crystallographic data in CIF format for compounds **1**−**3**, LeBail refinement of the powder spectrum of **4** (Figure S1), M vs H/T plot for **2** (Figure S2), M vs H/T and M vs H plots for **3** (Figure S3). This material is available free of charge via the Internet at http://pubs.acs.org.